Journal of Physics D:
Applied Physics

PAPER

A sound insulation cooling fin for broadband noise control and ventilation

To cite this article: Weiwei Liao *et al* 2025 *J. Phys. D: Appl. Phys.* **58** 085502

IOP Publishing Journal of Physics D: Applied Physics
J. Phys. D: Appl. Phys. **58** (2025) 085502 (11pp) https://doi.org/10.1088/1361-6463/ad9bc6

A sound insulation cooling fin for broadband noise control and ventilation

Weiwei Liao, Jia Hao and Xiaobing Luo*

School of Energy and Power Engineering, Huazhong University of Science and Technology, Wuhan 430074, People's Republic of China

E-mail: luoxb@hust.edu.cn

Received 24 October 2024, revised 25 November 2024
Accepted for publication 9 December 2024
Published 18 December 2024

Abstract

The noise generated by the ultrathin centrifugal fan in a laptop can significantly impact user comfort. While optimizing the fan itself for noise control is important, addressing noise propagation is also crucial. Due to space limitations inside a laptop, adding an extra component for noise control is nearly impossible. Therefore, modifying the cooling fin outside of the fan outlet for sound insulation can be an effective solution. A sound insulation cooling fin is proposed to provide broadband noise insulation while maintaining proper ventilation. Through the introduction of a coupled area change passage, noise at specific frequencies at the passage outlet can be managed to be insulated due to the destructive interference. The effectiveness of the unit's sound insulation is verified through an impedance tube measurement. Moreover, combining different units can create a multi-peak sound insulation effect which is suitable for various noise conditions. To meet the demand of real situations, a reversal design flow combining neural network and nonlinear constrained optimization algorithm is developed. As a result, a sound cooling fin combing 2 sound insulation units featuring 4013 Hz and 6000 Hz is fabricated and the actual insulation performance is measured in an anechoic chamber. The sound transmission loss at the designed frequency range reaches 5 dB, aligning well with the simulation results. The sound insulation cooling fin has the potential to be widely used for noise control in small-scale electronic devices.

Keywords: noise control, sound insulation, cooling fin, ventilation

1. Introduction

As the electronic devices are getting thinner and compact, the thermal management system has adjusted to the extreme installation space. Multiple ultrathin heat pipes combine to transfer heat from the chip to the cooling fin and an ultrathin centrifugal fan blows the heat into the environment. With the increasing power of heat generation, the centrifugal fan must increase the revolutionary speed to improve the convection rate, resulting in a corresponding increase in the sound pressure level. Hence, in laptops, the noise of the centrifugal fan poses a significant challenge as there are various operational conditions with different sound characteristics. Aiming at the critical noise problem, different methods to reduce the noise level are being considered. Except the biomimetic design to reduce the noise level from the source [1], this paper focuses on noise control along the sound propagation route.

Regarding the noise control method on the propagation route, there are two primary approaches: noise insulation [2–5] and noise absorption [6, 7]. They have different noise reduction mechanisms. Noise insulation reduces sound transmission mainly by the blocking effect of the material itself or the wave interference, whereas noise absorption reduces sound radiation mainly through standing wave resonation and dissipating the sound energy to the heat energy.

In terms of sound insulation, there are different types of acoustics metamaterials, among which membrane-type acoustic metamaterials [8, 9] and plate type metamaterials [10, 11] are widely utilized in low-frequency sound insulation. In

* Author to whom any correspondence should be addressed.

addition, there are various applications such as combining with a Helmholtz resonator [12] or with a plate-type chamber [13]. This paper reviews all the modifications on the membrane-type sound insulation acoustics metamaterials [11]. Moreover, using the wave interference mechanism to block sound waves has been proven to be efficient for sound insulation with perforated plates and membranes [14]. The membrane type and its modified metamaterials do show its advantage in low-frequency and broadband noise insulation. However, it is not suitable for the application inside the laptop since there is a need for air ventilation and extreme installation space.

Considering air ventilation application, some works are conducted to grant the metamaterial features of air ventilation [15–17]. Fano resonances are usually used to design broadband sound insulation metamaterials [18–21]. A similar destructive interference mechanism is also used to block sound waves. An ultrathin ventilation metamaterial is developed and it is referred to as perforated and constrained acoustics metamaterial [22]. The ventilation ratio is restricted by the central air passage area. A highly sparse acoustic meta–insulator array with 20 units can achieve ventilated sound insulation for nearly 1 octave with 70% sparsity [23]. A similar square-shaped unit with side slits is developed and it can achieve omnidirectional insulation [24]. The latest research [25, 26] develops a metasurface muffling coating for pipeline ventilation and noise reduction, which is attached on the inner surface of the pipe along streamwise direction. The ventilatable area accounts for 55.5% of the section area and the highest sound transmission loss (STL) reaches 54.6 dB. However, the existing acoustic metamaterials for air ventilation still do not have enough air ventilation rate because the sound insulation metamaterials should be near the fan outlet and the low ventilation area will cause high flow resistance and deteriorated heat dissipation effect.

To deal with the noise problem in the ultrathin thermal management system, the fact that the noise characteristics are constantly changing to fit the changing heat dissipation burden should be considered. Hence, the characteristic frequency of the acoustics metamaterial should be designable and broadband. There are also tunable acoustics metamaterials for the scenarios where the noise is changing [16, 27]. A self-adaptive sound absorber, equipped with a feedback circuit, can adjust the slider and change the absorption frequency according to the noise signal [28]. A multi-functional acoustic metamaterial is proposed to achieve broadband noise insulation and switchable transmission [29]. This work develops a combination of Helmholtz resonator and microperforated panel to cater to the insulation of sound at different frequency ranges [30]. Mpps is used to control a two-stage centrifugal compressor noise radiated from the outlet [31].

In conclusion, to deal with the noise problem in small-scale electronic devices, acoustic metamaterials should have small dimensions, high ventilation, broadband insulation and customizable for different practical scenes at the same time. Most importantly, in small-scale electronic device, the cooling fin is mounted closely to the outlet of the ultrathin centrifugal fan and there is not any extra space in a laptop for any other new structure. Hence, it will be beneficial to make modifications directly on the cooling fin and have as little influence as possible on the flow and heat characteristics.

In the paper, a new structure based on the cooling fin is proposed. In this case, 1-fold and 2-fold insulation units are proposed to control the noise radiated from centrifugal fans in small-scale electronics, such as laptops. To deal with the multiple tones of the noise spectrum, the insulation unit can be superimposed to form broadband insulation. The simulation based on pressure acoustics is validated by the impedance tube measurement. The design flow combining the neural network and the nonlinear constrained algorithm is developed to design the insulation units according to the needed frequency. In addition, the flow effect on the insulation performance is also studied using the linear Navier–Stokes equation and the practical insulation performance of a sound insulation cooling fin is validated by the anechoic chamber.

2. Structural description

There are two types of sound insulation units, which are shown in figures 1(a) and (b) respectively. They are referred to as 1-fold and 2-fold type. 1-fold represents the unit that there is only a one-time area change in the wave advance route. 2-fold represents the unit that there are 2 times for area change. In 1-fold and 2-fold units, there exist wide channels and narrow channels. W_{narrow} represents the narrow channel width and W_{wide} represents the wide channel width. L_{narrow} and L_{wide} are the length parameters of narrow and wide channels respectively. In addition, the area change ratio is defined to be the ratio W_{wide} over W_{narrow}. The total length of the insulation is a key factor and it is defined to be the sum of L_{narrow} and L_{wide} in the case of 1-fold type and 2 times of L_{narrow} plus L_{wide} in the case of 2-fold type.

The basic mechanism for the insulation is the destructive interference that occurs at the outlet of the insulation unit. When the sound wave impinges on the insulation unit inlet, the sound wave is separated into 2 traveling sound waves and they enter the passages separated by the folded fin. The 2 separating sound waves experience different area change processes and this will induce the phase difference between the 2 traveling sound waves. When the sound waves arrive at the outlet, the phase difference of the sound waves at a specific frequency will induce destructive interference, thus insulating sound at a specific frequency.

The key parameters of defining the insulation frequency and the peak STL at characteristics frequency is are the area change ratio and the total length of the insulation unit. The relation between the structural parameters and the sound insulation performance will be explored in the following sections.

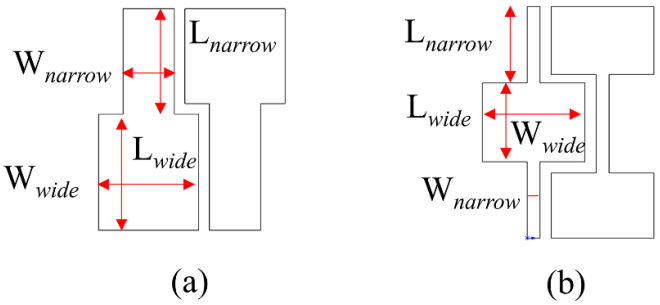

Figure 1. Structural dimension of insulation unit (a) 1-fold type (b) 2-fold type.

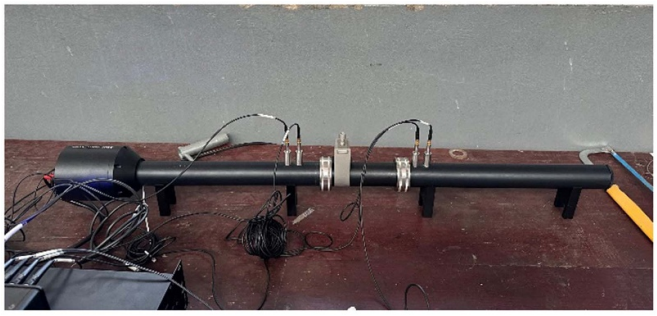

Figure 2. 4-microphone impedance tube.

3. Simulation and experimental method

3.1. Simulation method

3.1.1. COMSOL simulation. When the flow effects on sound transmission is neglected, the sound transmission can be simulated with the pressure acoustics method. The wave equation in the frequency domain can be reduced to equation (1),

$$\nabla \cdot \left(-\frac{1}{\rho_c} \left(\nabla p_t - q_d \right) \right) - \frac{k_{eq}^2 p_t}{\rho_c} = Q_m \tag{1}$$

$$p_t = p_3 + p_b \tag{2}$$

$$k_{eq}^2 = \left(\frac{\omega}{c_c} \right)^2 \tag{3}$$

where ρ_c is the air density, p_b is background pressure, p_3 is the fluctuation pressure, p_t is the total pressure, q_d is the source intensity, and ω is the angular frequency, c_c is the sound velocity and k_{eq} is the wave number, Q_m is source term.

When the flow effects on sound transmission is considered, the linearized Navier–Stokes equation is used to simulate the wave transmission. The control equation in frequency domain is listed below:

$$i\omega\rho_t + \nabla \cdot (\rho_t u_0 + \rho_0 u_t) = M \tag{4}$$

$$\begin{aligned} &\rho_0 \left(i\omega u_t + (u_t \cdot \nabla) u_0 + (u_0 \cdot \nabla) u_t \right) + \rho_t (u_0 \cdot \nabla) u_0 \\ &= \nabla \cdot \sigma + F - u_0 M \end{aligned} \tag{5}$$

where ρ_t represents the fluctuation density, u_0 is the average velocity and u_t is the fluctuating velocity, σ is the viscous stress and F is the body force, M is the source term.

The COMSOL Multiphysics is used to simulate the sound transmission. The inlet and outlet are set to plane wave radiation. When the flow is simulated, the coupling between the linear Navier–Stokes module and the turbulent flow module is set to background fluid flow coupling. The k–ω SST turbulent model is used to simulate the flow field. Next, the flow field mesh information is mapped to the sound field mesh. Finally, the acoustic field is solved.

In addition, the perfect match layer (PML) layer is set at the inlet and the outlet to diminish the sound wave, which contains 8 layers of structured grids. The volume mesh of the flow field is unstructured grids. The flow field mesh contains 5 layers of boundary layer girds. The acoustic mesh size is set to a tenth of the minimum sound wave interested to fully resolve the sound field.

3.1.2. Neural network surrogate model and optimization algorithm. Neural network is a newly developed method to build the connection between the input and outputs and normally the connection is hard to describe by mathematical or physical model. In essence, the neural network is a black box surrogate model and can help the researchers to reduce the complexity for building the model.

Regarding the details of the neural network utilized in this work, there are 2 layers of neurons and the middle layer consists of 10 neurons. The training algorithm is Bayes regulation and the mean square error (MSE) of the surrogate model is evaluated to judge whether the neuron network is applicable. The training data set makes up 75% of the total data set and the rest data is used for test and validation.

The Fmincon function in Matlab is a nonlinear optimization which is used to search for the minimum under specified constraints. The algorithm is based on the interior point. Firstly, an initial starting point needs to be fixed. In each iteration, the gradient of the objective function and the objective function is evaluated and adjust the input variables to reduce the objective function. In addition, the users can use different optimization methods according to practical needs. When the convergence condition is met, the iteration is terminated.

Combing the NN surrogate model and the Fmincon optimization algorithm, the researchers can design the wanted sound insulation cooling fin based on the real application needs.

3.2. Experimental method

The 4-microphone impedance tube shown in figure 2 is used to test the sound insulation amplitude of the tested specimen. The test method is based on ASTM-E2611 [32]. The narrow tube is used and the diameter is 29 mm to expand the testing frequency range up to 6400 Hz. The one-load method is used

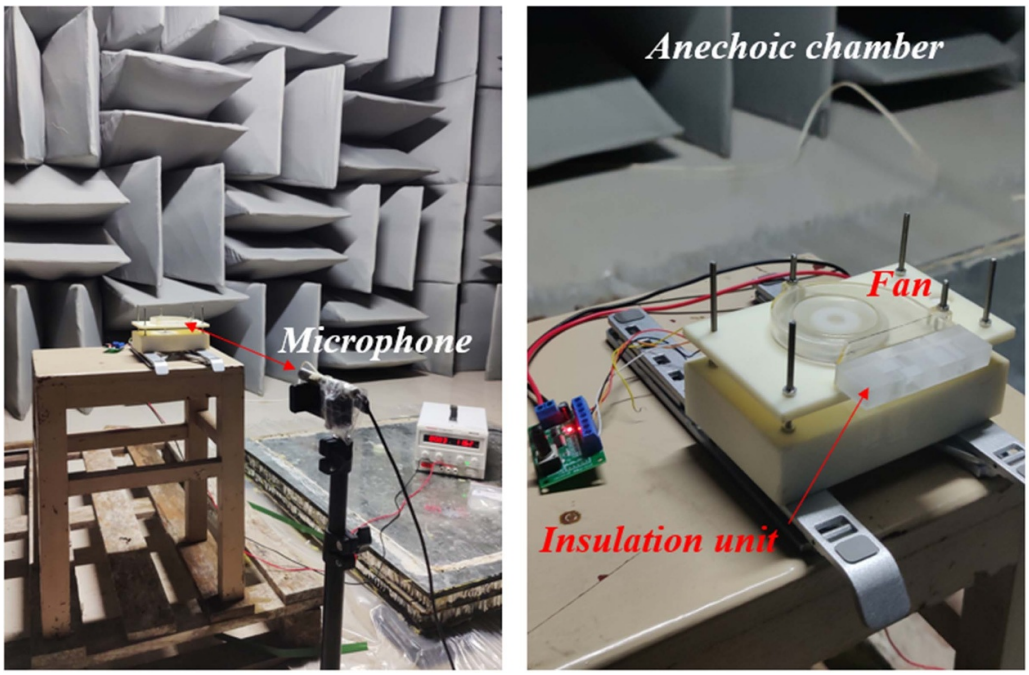

Figure 3. The experimental setup for the noise spectrum in an anechoic chamber.

and the terminal is set as an anechoic back. The transfer matrix is shown below:

$$T = \begin{bmatrix} \frac{p_d u_d + p_0 u_0}{p_0 u_d + p_d u_0} & \frac{p_0^2 - p_d^2}{p_0 u_d + p_d u_0} \\ \frac{u_0^2 - u_d^2}{p_0 u_d + p_d u_0} & \frac{p_d u_d + p_0 u_0}{p_0 u_d + p_d u_0} \end{bmatrix} \tag{6}$$

where p_0, u_0 are sound pressure and sound velocity at the inlet port, while p_d, u_d are the signals at the outlet port.

The transmission coefficient can be calculated as below:

$$t = \frac{2e^{jkd}}{T_{11} + \left(\frac{T_{12}}{\rho c}\right) + \rho c T_{21} + T_{22}} \tag{7}$$

where k is the wave number and d is the diameter of the impedance tube, and ρ is the air density and c is sound velocity.

The STL can be calculated as below:

$$\mathrm{STL} = 20\log_{10}\left|\frac{1}{t}\right|. \tag{8}$$

The semi-anechoic chamber is used to test the noise spectrum of the ultrathin centrifugal fan and the noise insulation performance of the insulation unit array. The sound source is placed in the center of the semi-anechoic room and the microphone is set 50 cm away from the fan outlet. To test the sound insulation performance of the cooling fin, the noise spectrum of centrifugal fan is measured with and without the cooling fin mounted to the fan outlet respectively just as figure 3 shows.

The microphone is GRAS 46 AE 1/2' free field microphone. The available frequency range is 3.15–10 kHz and the available SPL range from 18 to 138 dB. The maximum test frequency can be up to 10 240 Hz. The measurement duration time is 0.8 s and the frequency resolution is 1.25 Hz. The FFT window function is set to a Hanning window and the overlap ratio is set to 50%.

4. Experimental validation

To make sure the simulation results are reliable, 5 specimens of different configurations are tested. Their structures are shown in figure 4. As shown in figure 4, there are 3 kinds of samples to be tested and they are 1-fold 2 passages, 2-fold 2 passages and 2-fold 3 passages, respectively. There is only one area change in the single unit, which is referred to as 1-fold shown in figures 4(a) and (b). The single unit, referred to as 2 passages, contains 2 passages separated by 1 piece of folded fin. Its sound insulation characteristics are worth further investigation. Figures 4(c) and (d) are samples which are 2-fold 2 passages. Moreover, specimen E shown in figure 4(e) is built to demonstrate whether there is superimposing effect when there are multiple passages. The structural parameters of different specimens are presented in table 1.

As shown in table 1, samples A, B, C, and D are relatively simple and their narrow channel and wide channel have consistent dimensions. The sample E is relatively complex and it contains 3 passages. The first passage width changes from 2 to 5 mm and the second passage width changes from 3 to 6 mm and the third passage changes from 5 to 8 mm.

The comparison between simulation results and experimental results is illustrated in figure 5. The studied frequency ranges from 1000 to 6400 Hz. The COMSOL simulation results are depicted in rectangular dot solid line and the experimental results are depicted in solid line. The simulation insulation spectrum of different specimens is compared in figure 5(f) and there also exists a control group in which the sample only

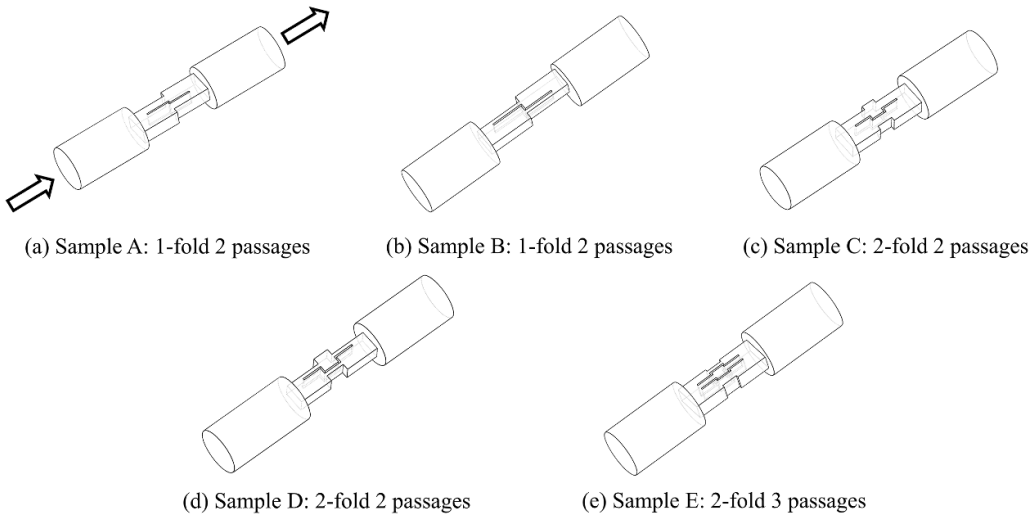

(a) Sample A: 1-fold 2 passages (b) Sample B: 1-fold 2 passages (c) Sample C: 2-fold 2 passages

(d) Sample D: 2-fold 2 passages (e) Sample E: 2-fold 3 passages

Figure 4. The tested specimen of different insulation units.

Table 1. Structural parameters of the test specimen.

	Sample A	Sample B	Sample C	Sample D	Sample E
W_{narrow}	5 mm	2 mm	5 mm	2 mm	2 mm/3 mm/5 mm
W_{wide}	10 mm	10 mm	8 mm	10 mm	5 mm/6 mm/8 mm
L_{narrow}	16 mm	21 mm	11 mm	13 mm	10 mm
L_{wide}	14 mm	19 mm	8 mm	10 mm	10 mm
Slit width	1 mm				
Silt height	10 mm				

has area change but does not have the interference. The control group has an insulation effect range from 1000 to 3000 Hz which is a descending slope and this is observed in the cases of every sample. Hence, it can be concluded that the insulation effect range from 1000 to 3000 Hz has nothing to do with sound wave interference.

As depicted in figure 5, the simulation results coincide well with experimental results, indicating the simulation method is reliable. Furthermore, different configurations of the tested specimens have different sound insulation characteristics. In terms of 1-fold samples, sample B has a larger area change ratio compared with sample A and sample B demonstrates a relatively lower peak frequency. The sample B also has a greater length than sample A. This indicates a larger area change ratio and longer travel distance may contribute to a lower insulation frequency, which needs further investigation. In terms of 2-fold samples, sample D has a larger area change ratio but a shorter length than sample C. As a result, sample D has an insulation frequency of as low as 3000 Hz. This phenomenon leads to the conclusion that a larger area change ratio contributes to lower frequency.

Comparing the results between 1-fold and 2-fold specimens, it is obvious that samples C and D have lower peak frequency, indicating that increasing the number of area changes can lead to lower frequency insulation.

In terms of sample E, there are two peaks observed at 4400 and 5000 Hz, indicating the superimposing effect is realizable in the case of two units. This implies that we can get the interested sound insulation spectrum aiming at different situations. However, at the same time, the amplitude of sound insulation in sample E is relatively smaller, only 12 dB, which is worth further exploration.

Figure 6 presents the isosurface of total acoustic pressure at different frequencies at 4000, 4500 and 5000 Hz of sample A. As shown in figure 5(a), sample A has a peak insulation frequency of 4500 Hz. From figure 6(b), it is obvious that the sound wave at 4500 Hz cannot travel through the insulation unit since the plane wave fades at the outlet. However, in figures 6(a) and (c), the sound wave at 4000 and 5000 Hz can travel through the insulation unit but the outlet sound pressure is 0.074 and 0.647 Pa respectively. The body arrow's size is characterized by the acoustic velocity and we can see from figure 6(b) that the sound velocity direction is from the wide channel to the narrow channel and this is caused by the pressure gradient. The strong interference insulates the sound wave at a specific frequency.

Figure 7 presents the isosurface of total acoustic pressure at different frequencies at 4000, 4500 and 5000 Hz of sample E. As can be seen in figure 5(e), the sample E is a 2-fold 3-passage insulation unit and possesses 2 characteristic frequency peaks,

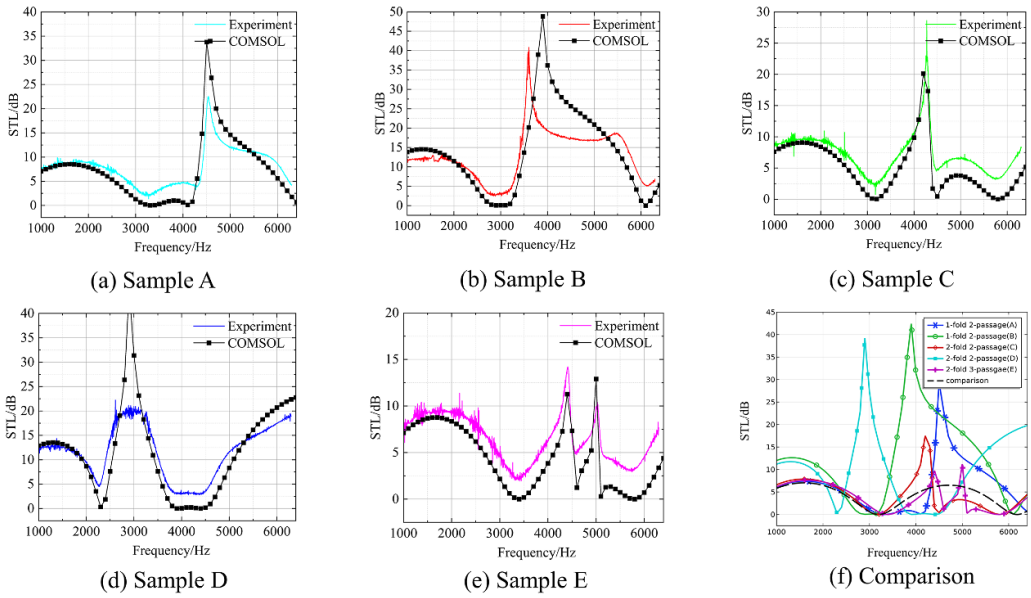

Figure 5. The insulation spectrum of different insulation units.

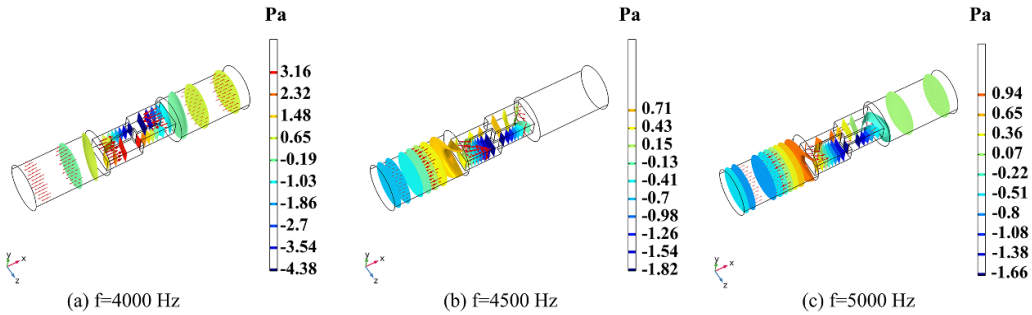

Figure 6. Isosurface of total acoustic pressure at different frequencies of sample A (a) 4000 Hz (b) 4500 Hz (c) 5000 Hz.

which are 4500 and 5000 Hz. At the frequency of 4000 Hz in figure 7(a), the insulation has little insulation effect. However, at 4500 and 5000 Hz, the sound wave cannot travel through the insulation unit but there is a difference. The characteristic frequency at 4500 Hz is caused by the interference of the left two channels while at 5000 Hz it is caused by the right two channels.

In conclusion, the simulation method is validated to be reliable. Furthermore, if an insulation unit with a lower insulation frequency needs to be designed, the area change ratio needs to be large and the total length should be long. More importantly, a multi-peak insulation unit can be obtained by superimposing two different units and this will help build a cooling fin which has broadband insulation.

5. Reversal design flow

We have demonstrated that the positive design flow is correct and accurate, but in the real situation, the reversal design method should be paid more attention. According to the noise spectrum of the specified noise source, it is necessary to design the sound insulation unit with the corresponding sound insulation frequency. To develop the reversal design flow, the neural network is adopted to get the surrogate model to predict the insulation peak frequency and its STL. Moreover, aiming at different units like 1-fold and 2-fold units, there need to develop different surrogate models. When the prediction model is obtained, the Fmincon nonlinear constrained optimization algorithm is used to get the structural parameters of the insulation units.

To get sparsely located data points in sampling space, the Latin hypercube sampling method is adopted. Regarding the 1-fold and 2-fold units, there are 4 input parameters. They are narrow channel width W_{narrow}, narrow channel length L_{narrow}, wide channel width W_{wide} and wide channel length L_{wide}. For a 2-fold channel, the narrow channel width is set to one fixed value for simplicity. Considering the real situation, the length of the cooling fin module is constant, meaning that the total length of wide and narrow channels is constant. In this case, the constant is set to 21 mm. There are a total number of 40 data points for the training of neural network and the values' range are listed in table 2.

The MSE of the neural network reaches 0.99, indicating that the neural network surrogate model can accurately predict the outputs according to the inputs. To further assess the

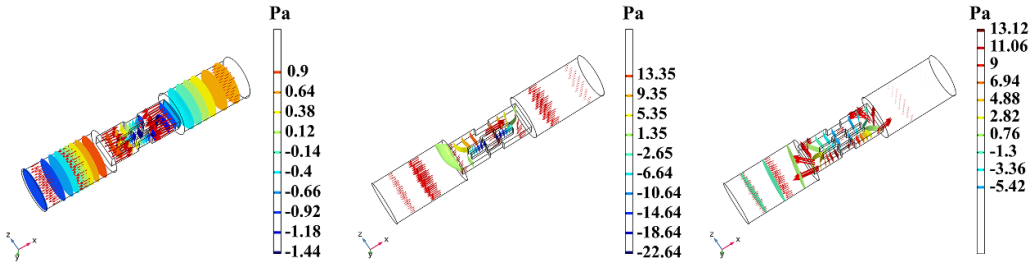

(a) f=4000 Hz (b) f=4500 Hz (c) f=5000 Hz

Figure 7. Isosurface of total acoustic pressure at different frequencies of sample E (a) 4000 Hz (b) 4500 Hz (c) 5000 Hz.

Table 2. Parameter value's range for Latin hypercube sampling.

	1-fold unit	2-fold unit
W_{narrow} (mm)	1–5	1–5
W_{wide} (mm)	6–10	6–10
L_{narrow} (mm)	8–12	6–8
L_{wide} (mm)	8–12	6–8
Constraint	$L_{\text{narrow}} + L_{\text{wide}} = 21$ mm	$2^{*}L_{\text{narrow}} + L_{\text{wide}} = 21$ mm

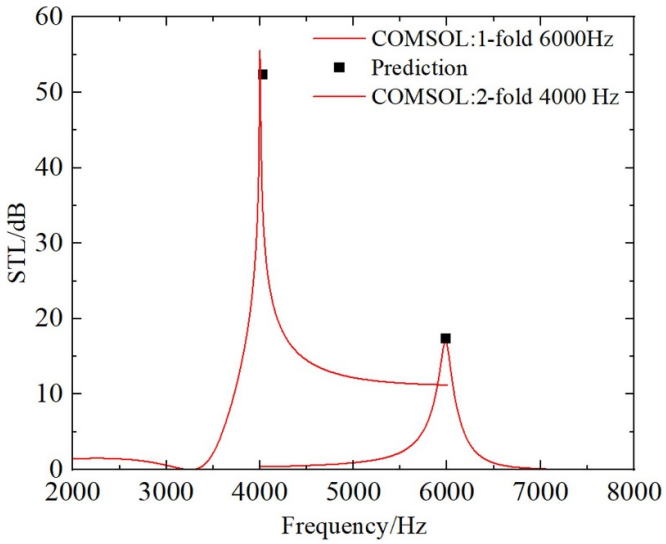

Figure 8. The comparison between the prediction and the simulation.

predictive accuracy of the surrogate model, two validation cases with objective frequencies of 4013 and 6000 Hz are utilized. The lower frequency corresponds to the 2-fold insulation unit, while the higher frequency is associated with the 1-fold insulation unit. In figure 8, the sound insulation spectrum of the simulation results is illustrated by a red solid line, and the NN's prediction of STL at the anticipated peak frequency is denoted by a black dot. It is evident from figure 8 that the prediction accuracy is satisfactory. The relative error of the STL remains within 5%, and the absolute error does not exceed 3 dB. The precision of the characteristic frequency prediction is of utmost importance, with the relative error falling within 1% and the absolute error not surpassing 50 Hz. Consequently, the forecast accuracy of the trained neural network is highly gratifying.

The training data is quite limited, yet the neural network demonstrates strong prediction accuracy. This can be attributed to the intrinsic relationship between the model's input parameters and the characteristic frequency. Despite there are 4 input parameters, the total length ($L_{\text{narrow}} + L_{\text{wide}}$) and the area change ratio ($W_{\text{wide}}/W_{\text{narrow}}$) are correlated with the characteristic frequency, as evident from the analysis of the various insulation units.

These two parameters' relation to the characteristic frequency in the case of 1-fold and 2-fold insulation units are depicted in figure 9. As shown in figure 9(a), red circle dots represent the area change ratio ($W_{\text{wide}}/W_{\text{narrow}}$) while black rectangular dots represent the total length ($L_{\text{narrow}} + L_{\text{wide}}$). It is noticeable that there exists a linear tendency between the input parameters and the frequency and they are marked by

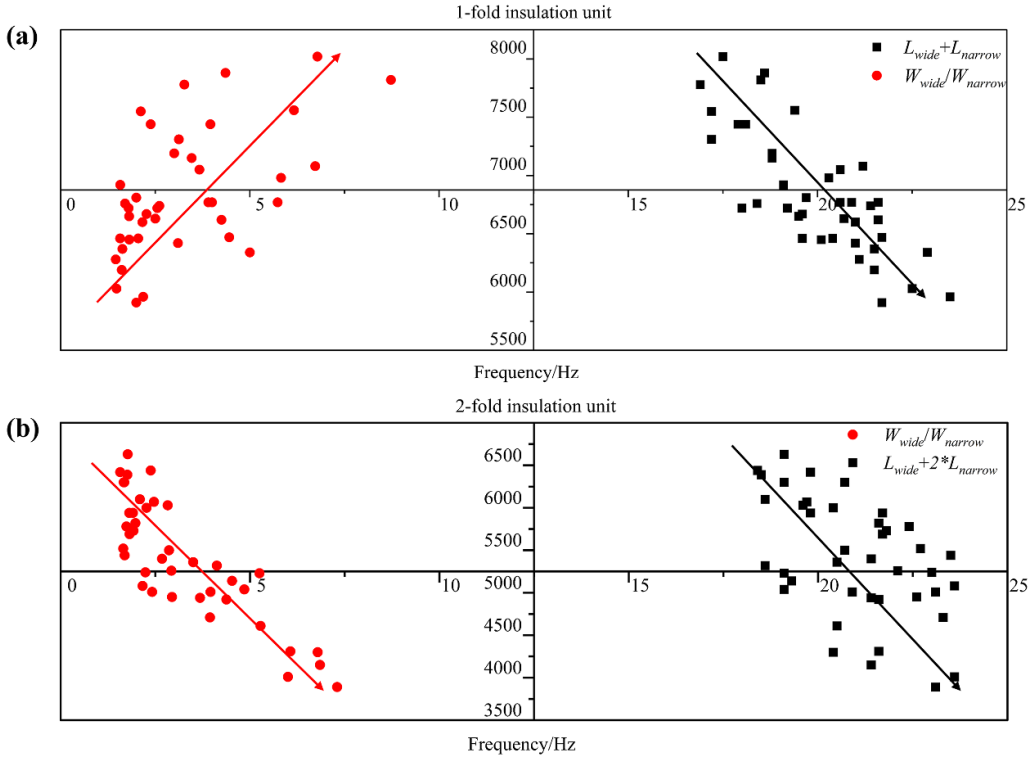

Figure 9. Relation between the area change ratio ($W_{\text{wide}}/W_{\text{narrow}}$), the total length ($L_{\text{narrow}} + L_{\text{wide}}$) and the characteristic insulation frequency in case of (a) 1-fold insulation unit (b) 2-fold insulation unit.

Table 3. The optimized model parameters.

	4013 Hz	6000 Hz
W_{narrow} (mm)	1.2	4.9
W_{wide} (mm)	9.3	9.6
L_{narrow} (mm)	6.9	10
L_{wide} (mm)	7.2	11

the red and black solid arrow line. Concretely speaking, the total length is inversely proportional to the characteristic insulation frequency while the area change ratio is proportional to it in the case of a 1-fold insulation unit. When a lower peak frequency is needed to be insulated, the corresponding insulation unit is better to be designed with a longer length and a small area change ratio.

In terms of the 2-fold insulation unit, the data points are depicted in figure 9(b). The only difference between the 1-fold insulation unit and the 2-fold insulation unit is the relation of the area change ratio to the characteristic frequency. In the case of a 2-fold insulation unit, when a lower frequency is needed, the area change ratio needs to be large. Hence, there exist different design patterns for 1-fold and 2-fold insulation units.

In addition, considering the real situation, the total length of the cooling fin is fixed. Consequently, the area change ratio is a good direction to be modified.

Now that the surrogate model is determined, to get the final parametric design, a solution algorithm is conducted. The objective function is modified to be the square of the difference between the objective frequency and the function so the Fmincon algorithm can search the minimum closer to 0 between the bounds. The start point is set to the lower bounds and the derivatives of the function and the constraints are both set to approximated by solver. The 4013 and 6000 Hz are set to be the design goal for the Fmincon algorithm and they are fit for 2-fold and 1-fold insulation units respectively.

After calculation, the model parameters are listed in table 3.

6. Results and discussion

6.1. Flow field analysis

The design flow is set so that we can design any insulation unit according to the objective frequency. In addition, the superposition of characteristic frequency has been proved and multi-peak insulation fins can be designed by the combination of different units. In this case, a multi-peak cooling fin has been fabricated with 4013 and 6000 Hz units combined. In addition, considering the real situation, the space between the 2 insulation units needs to be filled with straight channels. The structural model of the real cooling fin is depicted in figure 10(a).

The velocity and pressure distribution in the middle cutting plane in case of inlet velocity 5 m s^{-1} are presented in

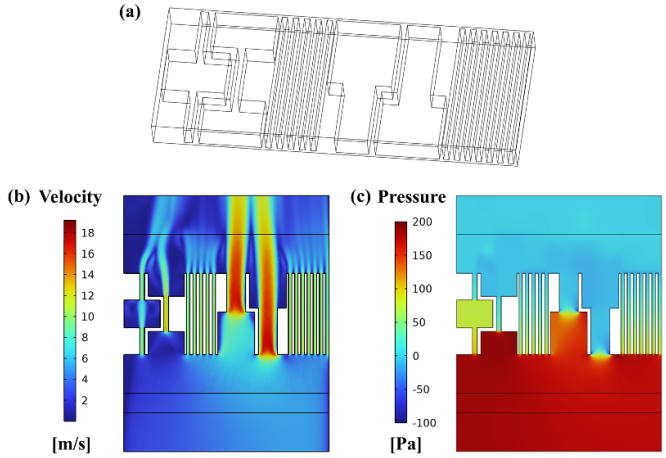

Figure 10. (a) The structural model of the combination of the designed 2-fold and 1-fold insulation units (b) velocity contour (inlet velocity 5 m s^{-1}) (c) pressure contour (inlet velocity 5 m s^{-1}).

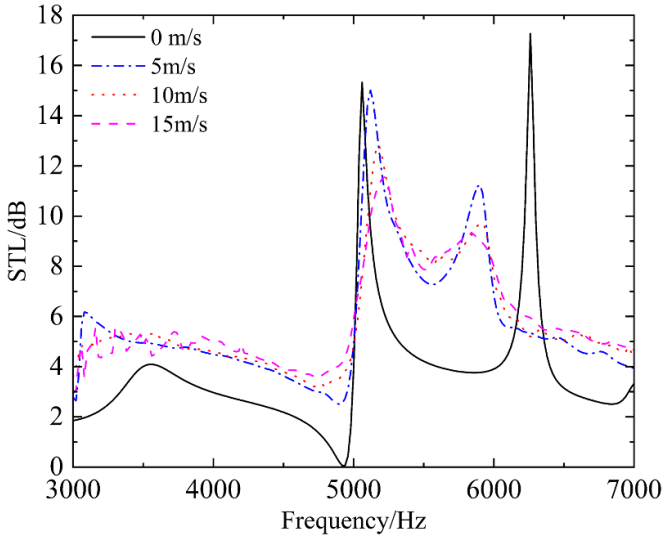

Figure 11. The simulation insulation spectrum of the combined insulation unit.

figure 10(b) and (c). The extended parts in the inlet are background pressure field and PML respectively and the extended part in the outlet is PML. As shown in the velocity and pressure field, the velocity increases when the pressure decreases, just as Bernoulli theorem indicates. In the section plane of 1-fold insulation unit where the channel area shrinks, it is noticeable that pressure will rise in a great extent and when the flow is over the plane, the pressure will decrease sharply. This reflects that the pressure loss in the kind of structure is large and the targeted measures should be done to optimize the flow loss and make sure the heat dissipation of the cooling fin is sustained to the maximum.

6.2. *Insulation analysis*

The insulation spectrums under different flow conditions are simulated and the results are shown in figure 11. From the spectrum under no flow condition, it is obvious that there are 2 distinct peak frequencies which are 5000 and 6300 Hz respectively and the insulation peak is so steep. Furthermore, the characteristic frequency of the combination of the insulation units is higher than the individual insulation unit. This phenomenon is also observed in sample E, from which we can deduce the combination of different units will shift the characteristic frequency to a higher range.

However, when there is airflow, the insulation spectra are quite different. When the inlet flow velocity is 5 m s^{-1}, the peak frequency at 6300 Hz shifts to 5800 Hz and the amplitude is reduced as well. The valley between the 2 peak frequencies has been filled up due to the existence of airflow. With the inflow velocity increases, the insulation spectrum did not change much. In conclusion, the airflow affects the insulation spectrum and is beneficial to form broadband insulation.

Mechanism analysis is necessary for why there exists peak frequency shifting and broadband formation. Given that the flow is quite slow and the Mach number is far smaller than 1, the sound wave propagation can be treated as adiabatic and there is no temperature gradient. Beyond that, the sound nonlinear effect can be neglected as well. The possible and reasonable explanation can be the boundary layer effect. The air impedance is changed due to the boundary layer thickness changing, inducing the change in the transmission and reflection features of the sound insulation unit.

The flow effect can do both positive and negative effect on the sound insulation performance of the acoustic metamaterial. For instance, a study demonstrated that as airflow velocity increased, the peaks at low frequencies in the STL curves decreased slightly but the insulation frequency band widened, indicating a positive influence on sound insulation under specific conditions [33]. It was also observed that the airflow will cause the shift of the resonance and the widening of the resonance peak [34]. In addition, in case of mufflers with various filling densities, the airflow increases the STL at lower frequencies in general, while for the mufflers with solid bulkheads or inlet tube, the airflow lowers the resonance intensity [35]. However, it was also observed that the airflow reduce the silencer attenuation [36].

In summary, the impact of airflow on the STL of acoustic metamaterials is nuanced. While some configurations can leverage airflow to enhance acoustic performance, others may suffer from reduced effectiveness due to complex interactions between sound waves and moving air.

The narrow band noise spectrum and 1/12 octave of the fan with and without the sound insulation cooling fin are illustrated in figure 12. The simulation results in figure 11 have shown that the insulation mainly works from 5000 to 6000 Hz when the flow is considered. As shown in figure 12(a), the noise level with the insulation unit is lower than that without the insulation unit, especially in the frequency range from 5000 to 6000 Hz. In addition, the noise level of the fan equipped with the sound insulation cooling fin from 4300 to 7000 Hz is approximately 5 dB lower and the effective range is consistent with the simulation results shown in figure 12(b).

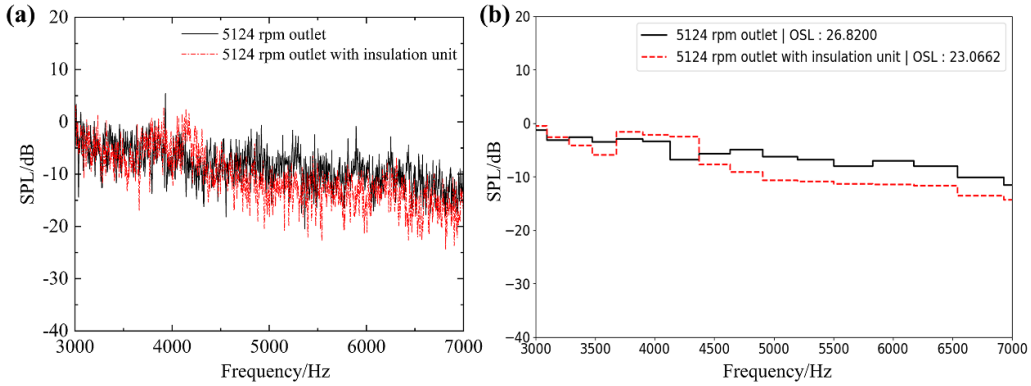

Figure 12. The noise spectrum comparison between the fan with and without the sound insulation cooling fin (a) narrow band (b) 1/12 octave.

In conclusion, the cooling fin has an insulation effect and its working frequency range is just as simulated and designed. The sound insulation cooling fin can be flexibly designed according to the varying noise conditions and achieve satisfying noise reduction effects.

7. Conclusion

To deal with the noise problem of the ultrathin centrifugal fan in small-scale electronics, a sound insulation cooling fin based on sound wave interference is proposed which can insulate noise in broadband frequency.

First, 5 different insulation units are fabricated and their insulation spectrum is measured by a 4-microphone impedance tube. The experimental results coincide with the simulation results well, validating the effectiveness of our simulation method.

Second, to handle the design problem in the real situation, a reversal design flow combining a neural network and a nonlinear optimization algorithm is proposed. The neural network prediction accuracy is satisfying and the reason for the accuracy with 40 training data sets is studied. This is mainly due to the intrinsic relation between the input parameters (area change ratio and total length) and output parameters (STL and characteristic frequency).

Third, a sound insulation cooling fin based on real needs is designed and fabricated to investigate the insulation performance in real situations. It combines 2 sound insulation units whose insulation peak frequency are 4013 Hz and 6000 Hz. In addition, its insulation performance under flow conditions is studied, revealing that the flow field can cause peak frequency shifting and contribute to forming broadband insulation. The sound insulation cooling fin is mounted at the outlet of the centrifugal fan and its noise spectrum is measured in an anechoic chamber. The experimental results show that the sound insulation cooling fin can decrease 5 dB in sound pressure level at the designed frequency range (5000–6000 Hz).

In conclusion, the sound insulation cooling fin has broadband insulation and its design flow is determined. Its flexibility in the frequency adjustment is essential for the changeable operation condition, meaning that this sound insulation cooling is usable in the noise reduction of small-scale electronic devices.

Data availability statement

All data that support the findings of this study are included within the article (and any supplementary files).

Acknowledgment

This research has been supported by the Open Fund of Science and Technology on Thermal Energy and Power Laboratory (No. TPL 2022B02).

Conflict of interest

The authors have no conflicts to disclose.

Author contributions

Weiwei Liao: Conceptualization(equal); Data curation(equal); Formal analysis(equal); Methodology(equal); Validation(equal); Writing-original draft(equal); Visualization(equal);

Jia Hao: Data curation(equal); Methodology(equal); Visualization(equal); Validation(equal);

Xiaobing Luo: Conceptualization(equal); Supervision(equal); Project administration(equal); Writing—Review & Editing(equal); Funding acquisition(equal).

ORCID iD

Xiaobing Luo https://orcid.org/0000-0002-6423-9868

References

[1] Sun Y, Li R, Wang L, Liu C, Yang Z and Ma F 2024 Bionic noise reduction design of axial fan impeller *J. Phys. Appl. Phys.* **57** 345501

[2] Cai T, Huang S, Guo H, Yuan T, Sun P and Liu N 2024 Sound insulation performance of membrane-type acoustic

metamaterial based on defect state structure *Phys. Scr.* **99** 025967
[3] Chen Z, Chong Y B, Lim K M and Lee H P 2024 Reconfigurable 3D printed acoustic metamaterial chamber for sound insulation *Int. J. Mech. Sci.* **266** 108978
[4] Zhang X, Zhao C, Wang P and Chen R 2024 Combined acoustic metamaterial design based on multi-channel Fano resonance effect *J. Appl. Phys.* **136** 013105
[5] Shen L, Zhu Y, Mao F, Gao S, Su Z, Luo Z, Zhang H and Assouar B 2021 Broadband low-frequency acoustic metamuffler *Phys. Rev. Appl.* **16** 064057
[6] Ma P-S, Kim H-S, Lee S-H and Seo Y-H 2022 Quasi-perfect absorption of broadband low-frequency sound in a two-port system based on a micro-perforated panel resonator *Appl. Acoust.* **186** 108449
[7] Liao W, Hu R, Xing G and Luo X 2023 Quasi-perfect and wideband absorption with gradient non-uniform micro-slit array absorber via a hierarchical optimization method *Appl. Acoust.* **206** 109321
[8] Peng W, Zhang J, Shi M, Li J and Guo S 2023 Low-frequency sound insulation optimisation design of membrane-type acoustic metamaterials based on Kriging surrogate model *Mater. Des.* **225** 111491
[9] Jang J-Y, Park C-S and Song K 2022 Lightweight soundproofing membrane acoustic metamaterial for broadband sound insulation *Mech. Syst. Signal Process.* **178** 109270
[10] Xiao Y, Cao J, Wang S, Guo J, Wen J and Zhang H 2021 Sound transmission loss of plate-type metastructures: semi-analytical modeling, elaborate analysis, and experimental validation *Mech. Syst. Signal Process.* **153** 107487
[11] Langfeldt F and Gleine W 2021 Plate-type acoustic metamaterials with strip masses *J. Acoust. Soc. Am.* **149** 3727–38
[12] Li H-Z, Liu X-C, Liu Q, Li S, Yang J-S, Tong L-L, Shi S-B, Schmidt R and Schröder K-U 2023 Sound insulation performance of double membrane-type acoustic metamaterials combined with a Helmholtz resonator *Appl. Acoust.* **205** 109297
[13] Wang X, Chen Y, Zhou G, Chen T and Ma F 2019 Synergetic coupling large-scale plate-type acoustic metamaterial panel for broadband sound insulation *J. Sound Vib.* **459** 114867
[14] Zhang Z, Wang X, Liu Z Y, Fan Q and Lin T R 2023 A study of low frequency sound insulation mechanism of a perforated plate-type acoustic metamaterial *J. Sound Vib.* **558** 117775
[15] Zhang X, Yu Q, Zhao C, Shi D, Geng M, Zheng J, Lu T and Wang P 2024 Modular reverse design of acoustic metamaterial and sound barrier engineering applications: high ventilation and broadband sound insulation *Thin-Walled Struct.* **196** 111498
[16] Li X, Zhang H, Tian H, Huang Y and Wang L 2022 Frequency-tunable sound insulation via a reconfigurable and ventilated acoustic metamaterial *J. Phys. Appl. Phys.* **55** 495108
[17] Yin Y-Q, Wu H-W, Cheng S-L, Sun W-J and Sheng Z-Q 2022 Acoustic metacage with arbitrary shape for broadband and ventilated sound insulation *J. Appl. Phys.* **132** 145101
[18] Xu Z, Qiu W, Cheng Z, Yang J, Liang B and Cheng J 2024 Broadband ventilated sound insulation based on acoustic consecutive multiple Fano resonances *Phys. Rev. Appl.* **21** 044049
[19] Dong R, Sun M, Mo F, Mao D, Wang X and Li Y 2021 Recent advances in acoustic ventilation barriers *J. Phys. Appl. Phys.* **54** 403002
[20] Xu Z, Zheng B, Yang J, Liang B and Cheng J 2021 Machine-learning-assisted acoustic consecutive Fano resonances: application to a tunable broadband low-frequency metasilencer *Phys. Rev. Appl.* **16** 044020
[21] Sun M, Fang X, Mao D, Wang X and Li Y 2020 Broadband acoustic ventilation barriers *Phys. Rev. Appl.* **13** 044028
[22] Wang X, Luo X, Yang B and Huang Z 2019 Ultrathin and durable open metamaterials for simultaneous ventilation and sound reduction *Appl. Phys. Lett.* **115** 171902
[23] Gao S, Zhu Y, Su Z, Zeng H and Zhang H 2022 Broadband ventilated sound insulation in a highly sparse acoustic meta-insulator array *Phys. Rev.* B **106** 184107
[24] He J, Zhou Z, Zhang C, Zheng Y, Li Y, Li Y, Jiang X and Ta D 2022 Ultrasparse and omnidirectional acoustic ventilated meta-barrier *Appl. Phys. Lett.* **120** 191701
[25] Liu Y, Zhang W, Cao G, Zuo G, Liu C and Ma F 2024 Ultra-thin ventilated metasurface pipeline coating for broadband noise reduction☆ *Thin-Walled Struct.* **200** 111916
[26] Liu Y, Cao G, Liu C and Ma F 2025 Ultra-thin arc-shaped conformal metasurface coating for broadband noise reduction in underwater pipeline *Appl. Acoust.* **228** 110314
[27] Nakayama M, Matsuoka T, Saito Y, Uchida N, Inoue K, Mitani H, Akasaka S and Koga S 2021 A practically designed acoustic metamaterial sheet with two-dimensional connection of local resonators for sound insulation applications *J. Appl. Phys.* **129** 105106
[28] Tian H, Xiang X, He K, Liu C, Hou S, Wang S, Huang Y, Wu X and Wen W 2021 Automatically adaptive ventilated metamaterial absorber for environment with varying noises *Adv. Mater. Technol.* **6** 2100668
[29] Xiao Z, Gao P, He X, Qu Y and Wu L 2022 Multifunctional acoustic metamaterial for air ventilation, broadband sound insulation and switchable transmission *J. Phys. Appl. Phys.* **56** 044006
[30] Su Z, Luo H, Gao S, Luo Z, Zhu Y and Zhang H 2022 Customizable acoustic metamaterial barrier with intelligent sound insulation *Phys. Rev. Appl.* **18** 064029
[31] Mao Y, Fan C, Zhang Z, Song S and Xu C 2021 Control of noise generated from centrifugal refrigeration compressor *Mech. Syst. Signal Process.* **152** 107466
[32] E33 committee test method for measurement of normal incidence sound transmission of acoustical materials based on the transfer matrix method
[33] Su Z, Zhu Y, Gao S, Luo H and Zhang H 2022 High-efficient and broadband acoustic insulation in a ventilated channel with acoustic metamaterials *Front. Mech. Eng.* **8** 857788
[34] Pak M C, Kim K-I, Pak H C and Hong K R 2021 Influence of geometric structure, convection, and eddy on sound propagation in acoustic metamaterials with turbulent flow *Arch. Acoust.* **46** 637
[35] Zhirong H, Zhenlin J and Yiliang F 2024 Acoustic attenuation prediction and analysis of perforated hybrid mufflers with non-uniform flow based on frequency domain linearized Navier-Stokes equations *Adv. Mech. Eng.* **16** 16878132231226055
[36] Sánchez-Orgaz E M, Denia F D, Martínez-Casas J and Baeza L 2014 3D acoustic modelling of dissipative silencers with nonhomogeneous properties and mean flow *Adv. Mech. Eng.* **6** 537935